Available online at www.sciencedirect.com
SCIENCE DIRECT®
Journal of the European Ceramic Society 25 (2005) 1389–1395
www.elsevier.com/locate/jeurceramsoc

# Microstructures and interfaces in directionally solidified oxide–oxide eutectics

Léo Mazerolles*, Daniel Michel, Martin J. Hÿtch

*Centre d'Etudes de Chimie Métallurgique—CNRS, UPR 2801, 15 rue G. Urbain, 94407 Vitry, Cedex, France*

Available online 30 January 2005

**Abstract**

This article reviews different studies carried out on the microstructures and oxide–oxide interfaces encountered in directionally solidified eutectics. Depending on the phase diagram and preparation conditions, lamellar, fibrous or three-dimensional network microstructures can be obtained. Interfaces between refractory oxides with various structural types (corundum, fluorite, rocksalt, perovskite and garnet) are investigated. Orientation relations and interface planes are reported and general features of the structure of interfaces are discussed from high-resolution electron microscopy (HREM) studies. The accommodation of lattice mismatch at the interface is investigated by geometric phase analysis of HREM images.


*Keywords:* Oxide; Interfaces; Electron microscopy

## 1. Introduction

In parallel to the improvement of mechanical properties of metallic systems in the field of advanced gas turbine blades, many ceramic eutectics are being studied because of their high melting points, high strength-to-weight ratios and resistance to oxidation. When grown under controlled solidification conditions, directionally solidified ceramic eutectics have useful intrinsic properties: low porosity, microstructural stability up to temperatures close to the eutectic temperature and good bonding between phases.[1–3] The phases are uniformly distributed and their spacing can be adjusted in order to limit the size of microcracks. In addition, they are free from transverse grain boundaries, which limit rupture strength.

The distribution and the structure of interfaces have a marked influence on the final properties. Consequently, it is of major interest to know how eutectic phases are accommodated at interfaces. This paper shows different types of microstructures that we obtained by various directional solidification techniques. Crystallographic relations between the two phases of eutectic structures will be reported. In addition, results of HREM observations of eutectic interfaces are presented and a new method for analysing defects at the interface by numerical treatment in Fourier space will be developed.

## 2. Experimental

Directionally solidified ceramic eutectics were prepared by the two following methods, also used to grow ceramic single crystals. Details of these techniques have been extensively reported in previous papers:[4–6]

(i) the "skull-melting" method consisting of radio frequency (RF) direct induction heating of powder mixtures in a water cooled-copper crucible. Directional solidification is obtained either by a slow cooling of the crucible content or by Czochralski pulling from the melt ingot.
(ii) a floating zone device associated with a double ellipsoid image furnace operating with a 6 kW xenon lamp as radiation source.

Both methods led to rods of oriented eutectics (diameter: 6–8 mm, length: 60 mm). Very similar microstructural and crystallographic features were obtained by these two ways of

* Corresponding author.
*E-mail address:* mazerolles@glvt-cnrs.fr (L. Mazerolles).

0955-2219/$ – see front matter © 2005 Elsevier Ltd. All rights reserved.
doi:10.1016/j.jeurceramsoc.2005.01.015

preparation. Solidification rates were varied between 2 and 20 mm $h^{-1}$.

The techniques are well adapted to the fabrication from the melt of aligned eutectic structures because they allow high $G/R$ values ($G$ is the temperature gradient at the solid-liquid interface and $R$ is the growth rate). Mollar and Flemings[7] have shown the existence of a critical ratio $(G/R)_c$ related to a plane-front growth which is required to obtain an aligned microstructure in binary systems. This value is dependent on the as-considered system. At eutectic composition, the $(G/R)_c$ value corresponds to a minimum and a planar liquid-solid interface can be obtained more easily, but plane-front growth conditions can also be achieved for off-eutectic materials far from the eutectic composition with a steep temperature gradient and a sufficiently slow growth rate.

The orientations of samples were determined from X-ray diffraction and electron diffraction in cross-sections. Platelets were cut perpendicularly to the growth direction for observations by transmission electron microscopy (TEM). Thinning was achieved by mechanical polishing followed by argon ionic bombardment in order to reach a final thickness of about 5–25 nm for the observed areas.

## 3. Microstructures and crystallography of interfaces

For low values of solidification rate corresponding to high $G/R$ ratios, oriented eutectic microstructures are either lamellar or fibrous. Cooksay et al.[8] calculated that the interfacial area per unit volume was lower for a fibrous microstructure when the minor-phase volume fraction is lower than 0.28. At higher minor-phase volume fractions, a lamellar structure is favoured. This fraction volume limit has been confirmed for several binary systems in the work of Minford et al.[9] who compiled the results relative to about 25 non-metallic eutectic structures. The microstructures that we have obtained on different systems are in good agreement with these results. In the $ZrO_2$–$Ln_2O_3$ (Ln: La, Nd, Dy), $ZrO_2$–MO (M: Mg, Ni), $ZrO_2$–$Al_2O_3$ systems, we have grown at eutectic composition directional microstructures consisting of parallel fibres or lamellae (Figs. 1 and 2).[5,10] In these systems, the variation of the interlamellar (or interfibre) spacing $\lambda$ with the growth rate $R$ follows a relation close to the $\lambda^2 R$ = constant proposed by Tiller[11] and developed by Hunt ad Jackson[12] and which is verified for most ceramic eutectics.[13,14] In some cases this lamellae–fibre transition can be modified by the anisotropy of surface energy. For example, a particular crystallographic orientation relation might result in a lower-surface-energy between the phases and favour a lamellar microstructure even for low values of the volume fraction of the minor constituent. On Fig. 3 is shown the transition between lamellae and fibres in the $ZrO_2$–MgO eutectic.

The presence of impurities or the addition of a third element (ternary systems) increases the $(G/R)_c$ value and consequently a cellular growth is frequently observed. We have effectively observed in the $Al_2O_3$–$ZrO_2$–$Y_2O_3$ ternary eutectic

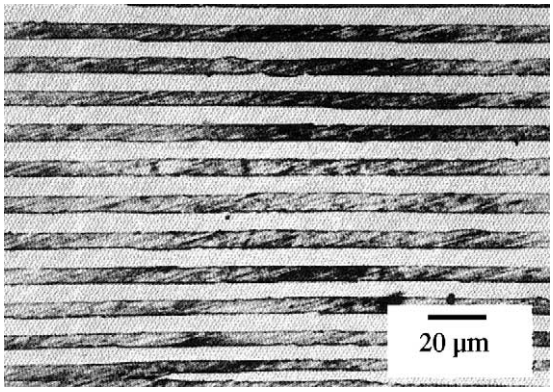


Fig. 1. $ZrO_2$–70 mol% $Nd_2O_3$ eutectic obtained at $R = 0.4$ cm $h^{-1}$. Alternate lamellae of $Nd_2O_3$ and $ZrO_2$ observed on a transverse section (optical micrograph).

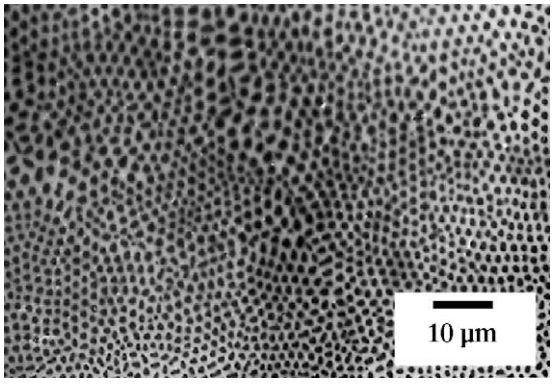


Fig. 2. $ZrO_2$–50 mol% MgO eutectic obtained at $R = 1.5$ cm $h^{-1}$. Optical micrograph of a transverse section showing MgO fibres oriented in a cubic zirconia matrix.

a "colony" structure (Fig. 4) with a microstructure consisting of cubic or tetragonal zirconia (depending on amount of yttria) particles in an alumina matrix.[10,15]

In addition to the eutectic microstructure, we observed, in some cases, secondary microstructures resulting from solid state transformations (eutectoid decomposition, phase transition). For example, in the $ZrO_2$–CaO lamellar eutectic,

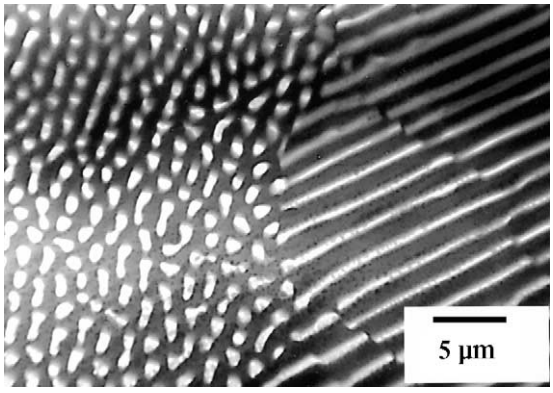


Fig. 3. $ZrO_2$–50 mol% MgO eutectic. MET image of the transition between lamellar and fibrous microstructures.

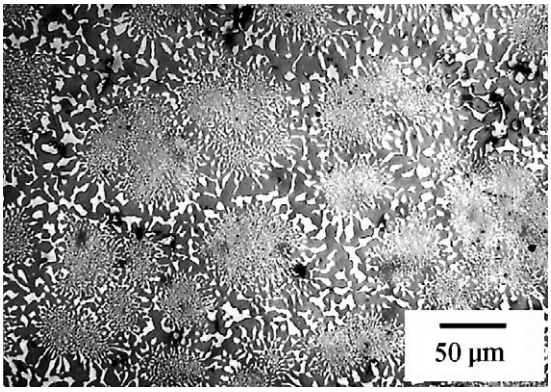


Fig. 4. 62 mol% $Al_2O_3$–34.5 mol% $ZrO_2$–3.5 mol%$Y_2O_3$ eutectic. Colonnar microstructure.

the $CaZrO_3$ phase, with the perovskite structure, undergoes through cooling a cubic → tetragonal transformation from the cubic prototype form (*Pm3m*, $Z = 1$) to the orthorhombic variety stable at room temperature (*Pnma*, $Z = 4$). Consequently, this transformation gives rise to a domain structure corresponding to variants produced by the symmetry lowering (Fig. 5).

More recently, others microstructures which do not correspond to aligned or colonnar microstructures have been obtained by directional solidification. These microstructures consist of three-dimensionally continuous and complexly entangled single-crystal eutectic phases.[16–18] We have prepared these types of microstructures in various systems associating alumina with perovskite or garnet structures (Fig. 6a). The highly interconnected character of phases in these systems is a promising factor concerning the increase of fracture toughness by crack deflection mechanisms. An example is given on Fig. 6b showing changes of directions of a crack at the interface between two phases, which do not display the same mechanical behaviour.

Some years ago, crystallographic data on oxide–oxide eutectics in binary systems were reviewed by Minford et al.[9] and by Revcolevschi et al.[19] Results obtained on composites studied in our laboratory are gathered in Table 1. In all cases,

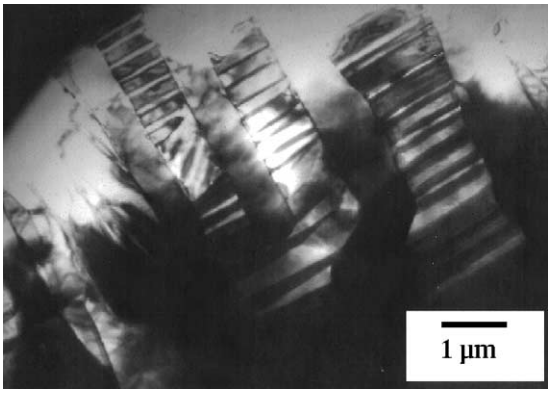


Fig. 5. $ZrO_2$–$CaZrO_3$ eutectic ($ZrO_2$–40 mol% CaO). MET micrograph of variants in the $CaZrO_3$ phase.

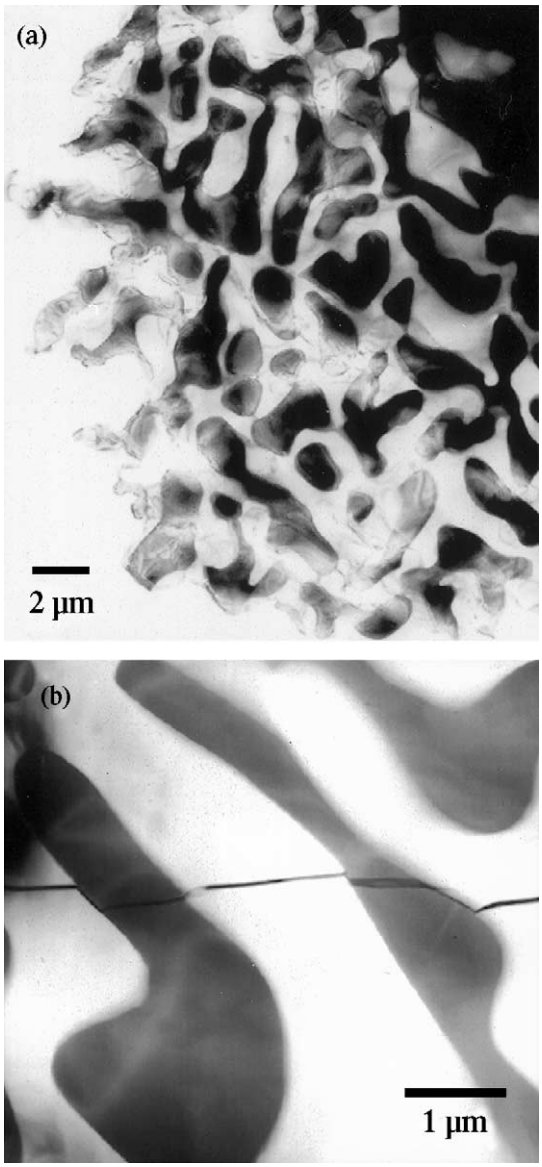


Fig. 6. Three-dimensional network microstructures between (a) $GdAlO_3$ (dark contrast) and $Al_2O_3$ (bright contrast) phases at the eutectic composition $Al_2O_3$–23 mol% $Gd_2O_3$. (b) $Er_3Al_5O_{12}$ (dark contrast) and $Al_2O_3$ (bright contrast) phases at the eutectic composition $Al_2O_3$–19 mol% $Er_2O_3$. Propagation of a microcrack.

growth axes correspond to well-defined crystallographic directions. The following remarks can be made from these experimental results:

- in most cases the growth direction and crystallographic orientation relations are unique. However, two different growth directions are sometimes found for one set of relative orientations of eutectic phases ($Al_2O_3$–$ZrO_2$ eutectic).
- interface planes have low Miller indices and constituent phases are perfectly aligned within ±1° (Fig. 7). Generally these planes correspond to dense arrangements of atoms as for instance the $(1\,\bar{1}\,1)$ plane for phases with a fcc lattice and $(0\,0\,0\,1)$ or $(2\,0\,\bar{1})$ for $Ln_2O_3$ compounds with A and B type structures.

Table 1
Crystallographic data relative to various oxide–oxide interfaces

| Coupled structures | Phases | Growth direction | Interface planes |
|---|---|---|---|
| Corundum–fluorite | $Al_2O_3$–$ZrO_{2cub}$ | $[0\,0\,0\,\bar{1}\,1]Al_2O_3//[0\,1\,0]ZrO_2$; $[0\,1\,\bar{1}\,0]Al_2O_3//[0\,0\,1]ZrO_2$ | $(2\,\bar{1}\,\bar{1}\,0)Al_2O_3//(1\,0\,0)ZrO_2$ |
| Fluorite–perovskite | $ZrO_2$–$CaZrO_3$ | $[1\,1\,0]ZrO_2//[0\,1\,\bar{1}]CaZrO_3$ | $(1\,\bar{1}\,0)ZrO_2//(1\,0\,0)CaZrO_3$ |
| Corundum–perovskite | $Al_2O_3$–$GdAlO_3$ | $[0\,1\,\bar{1}\,0]Al_2O_3//[1\,\bar{1}\,0]GdAlO_3$ | $[2\,\bar{1}\,\bar{1}\,0]Al_2O_3//[1\,1\,2]GdAlO_3$ |
| Spinel–rocksalt | $MnAl_2O_4$–MnO | $[1\,\bar{1}\,1]MnAl_2O_4//[1\,1\,1]MnO$ | $(h\,k\,l)MnAl_2O_4//(h\,k\,l)MnO$ |
| Fluorite–rocksalt | $ZrO_2$–MO (M: Mg, Ni) | $[1\,\bar{1}\,0]ZrO_2//[1\,\bar{1}\,0]MO$; $[0\,1\,\bar{0}]ZrO_2//[1\,\bar{1}\,\bar{0}]MO$ | $(1\,1\,1)ZrO_2//(1\,1\,1)MO$; $(1\,0\,0)ZrO_2//(1\,1\,1)MO$ |
| Fluorite–$Ln_2O_3$ (A) | $ZrO_2$–$Nd_2O_3$ | $[1\,\bar{1}\,0]ZrO_2//[2\,\bar{1}\,\bar{1}\,0]Nd_2O_3$ | $(1\,1\,1)ZrO_2//(0\,0\,0\,\bar{1}\,1)Nd_2O_3$ |
| Fluorite–$Ln_2O_3$ (B) | $ZrO_2$–$Sm_2O_3$ | $[1\,\bar{1}\,0]ZrO_2//[1\,\bar{3}\,2]Sm_2O_3$ | $(1\,\bar{1}\,1)ZrO_2//(2\,0\,\bar{1})Sm_2O_3$ |
| Corundum–mullite | $Al_2O_3$–$Al_6Si_2O_{13}$ | $[0\,0\,0\,1]Al_2O_3//[0\,0\,1]mul.$ | $(2\,\bar{1}\,\bar{1}\,0)Al_2O_3//(1\,0\,0)mul$ |

$Ln_2O_3$ (A), trigonal; $Ln_2O_3$ (B), monoclinic.

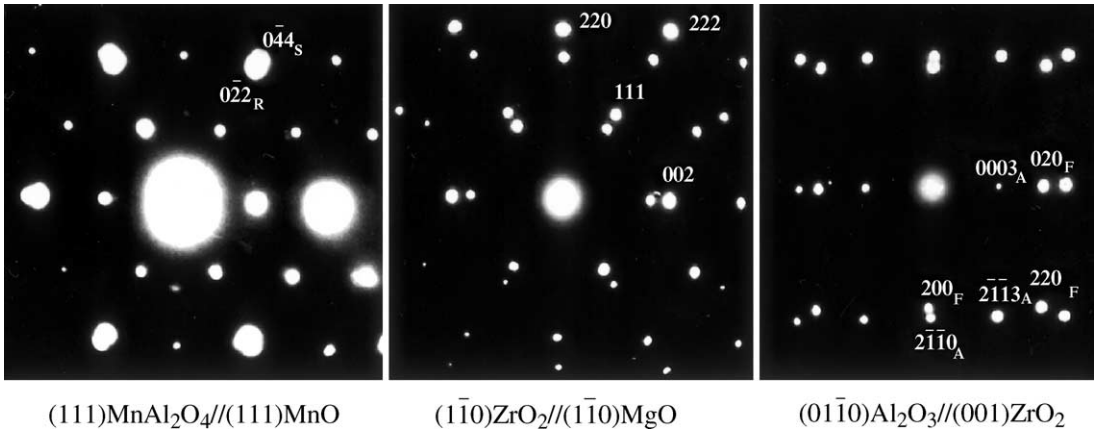


Fig. 7. TEM diffraction patterns of interface areas including spots of both phases (S, spinel; R, rocksalt; F, fluorite; and A, alumina) obtained on transverse sections of various eutectics.

- in fibrous eutectics, the growth direction seems to be governed by the matrix only since this axis is the one that is usually observed during growth of single crystals of the major phase. The same feature is observed in 3D microstructures where the growth direction is imposed by the major phase (Fig. 8).
- in lamellar eutectics, the solidification axis is a direction of easy growth contained in the interface plane, but is not necessarily the preferred growth direction of constituent phases.

## 4. Study of interfaces at atomic scale

In the previous section we showed that the microstructure is oriented along preferred crystallographic directions. Consequently the two constituent phases are perfectly oriented along dense atomic rows, which allows a correct imaging on both sides of the interface for high-resolution electron microscopy (HREM) observations. Therefore, edge-on examination of interfaces can be directly carried out on transverse sections of oriented eutectics.

HREM studies show that the thickness of these interfaces does not exceed 0.5 nm. Usually, the change from one phase to the other occurs on one or a few interatomic distances only. The coherency relations between coupled structures clearly appear on HREM images.[20–22] Two examples are given on Figs. 9 and 10. On Fig. 9, interface between $ZrO_2$ dispersoids and the $Al_2O_3$ matrix is exhibited. The lattice coincidence between zirconia and alumina is visualized by a periodic alignment of $(0\,0\,0\,1)Al_2O_3$ and $(0\,1\,0)ZrO_2$ planes. Five interplanar spacings in zirconia ($5 \times a/2 = 1.29$ nm) are nearly equal to three in alumina ($3 \times c/3 = 1.3$ nm). Fig. 10 concerns an interface between magnesia and zirconia. The $ZrO_2$–MgO eutectic generally consists of magnesia fibres aligned in a fluorite-type zirconia matrix[23] with the $[h\,k\,l]MgO//[h\,k\,l]ZrO_2$ orientation relation. Magnesia fibres are well-aligned along the direction $\langle 1\,1\,0\rangle MgO//\langle 1\,1\,0\rangle ZrO_2$ and have $\{1\,1\,0\}$, $\{0\,0\,1\}$ and $\{1\,1\,1\}$ lateral faces. The difference between unit-cell parameters of the two cubic phases is about 20%. Coherency relations between magnesia and zirconia rows are restored by an array of periodic misfit dislocations corresponding to the insertion of one additional $\{1\,1\,1\}$ magnesia plane for each five $\{1\,1\,1\}$ zirconia planes ($5aZrO_2 = 6aMgO$ within 0.1%).

In some cases a slight misorientation between phases at the interface occurs. The high-resolution image shown on Fig. 11a is an illustration of this case. The transverse section exhibited on this figure comes from another growth direction

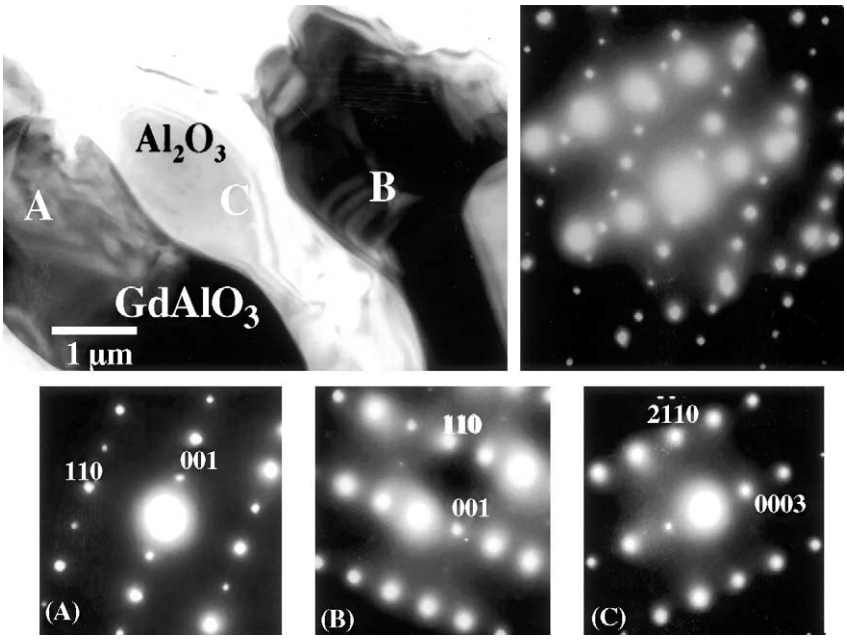


Fig. 8. TEM image and diffraction patterns relative to the $Al_2O_3$–$GdAlO_3$ eutectic. The A–C letters show the areas selected for the diffraction patterns presented below. The SAD pattern on the right of the image corresponds to the interface A–C.

of the $Al_2O_3$–$ZrO_2$ eutectic but the orientation relation between phases is the same as this one shown on Fig. 9. The hexagonal symmetry of the [0 0 0 1] projection of corundum and the four-fold symmetry of [0 1 0] fluorite are imaged on both sides of a $\{2\,\bar{1}\,\bar{1}\,0\}Al_2O_3//\{1\,0\,0\}ZrO_2$ interface. In order to reach a better definition of the interface we applied geometric phase analysis on this HREM image.

The geometric phase technique was designed to measure the displacement of lattice fringes from high-resolution images.[24] However, it can also be used for measuring the precise orientation of crystals and detecting interfacial dislocations.[25] The phase refers to the local phase difference between interference fringes in an image and a perfectly periodical reference lattice. The phase is directly related to the displacement field and the phase gradient indicates a change in lattice spacing or orientation. The first step is to calculate the Fourier transform of the image (Fig. 11b) and to choose the image periodicities to analyse via a mask. Traditionally, a single set of interference fringes is chosen but for the case of heterophase interfaces, a periodicity present on each side of the interface can be chosen within the mask.[26] The resulting phase image is shown in Fig. 11b for the 0 0 2 and $\bar{1}\,2\,\bar{1}\,0$

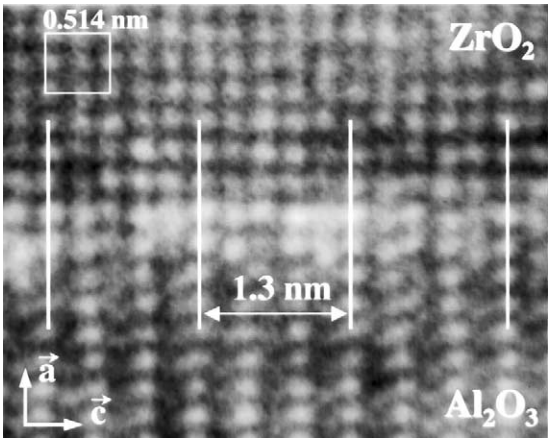


Fig. 9. HREM image of a transverse section of a $[0\,1\,\bar{1}\,0]Al_2O_3$–$[0\,1\,0]ZrO_2(Y_2O_3)$ eutectic. Edge view of a $\{2\,\bar{1}\,\bar{1}\,0\}Al_2O_3//\{1\,0\,0\}ZrO_2$ planar interface.

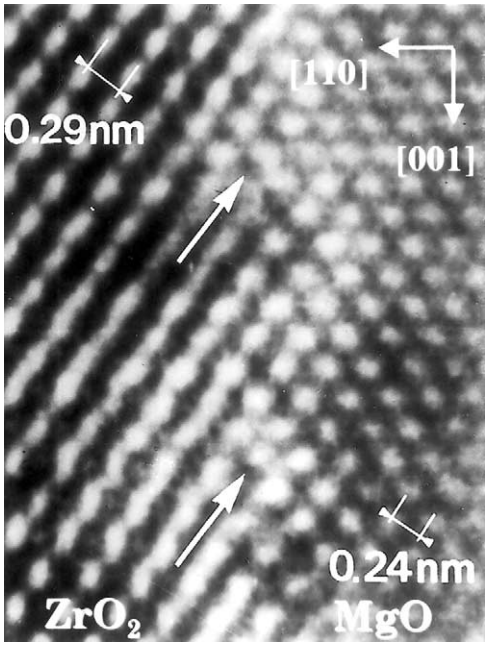


Fig. 10. HREM image of a transverse section of an oriented $[1\,1\,0]ZrO_2$–$[1\,\bar{1}\,0]MgO$ eutectic.

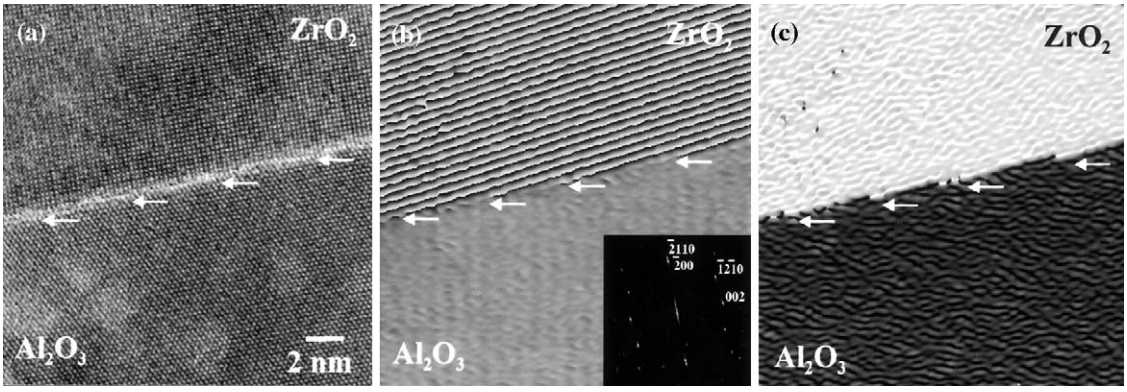


Fig. 11. (a) HREM image of a transverse section of a [0 0 0 1]$Al_2O_3$–[0 1 0]$ZrO_2(Y_2O_3)$ eutectic. Edge view of a $\{2\,\bar{1}\,\bar{1}\,0\}Al_2O_3//\{1\,0\,0\}ZrO_2$ planar interface. (b) Phase image (the white arrows indicate discontinuities of phase revealing steps; the power spectrum of the HR image is shown in inset). (c) Phase gradient image.

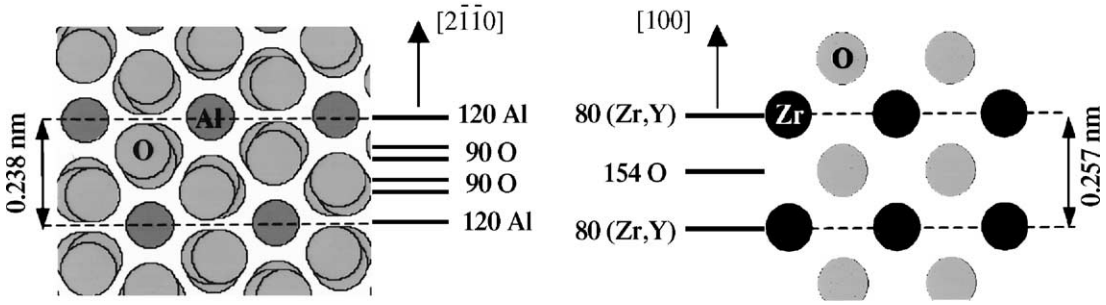


Fig. 12. Atomic stacking on both sides of the $Al_2O_3$–$ZrO_2(Y_2O_3)$ eutectic interface: $\{2\,\bar{1}\,\bar{1}\,0\}Al_2O_3//\{1\,0\,0\}ZrO_2$.

lattice fringes, with the reference chosen in alumina. The difference in gradient from one side of the interface to the other, which produces the series of black lines, gives the change in the reciprocal lattice vector in exactly the same way as for moiré fringes. By measuring the gradient, the orientation relation can be precisely determined. In this case there is a slight misorientation of 0.4° between the ($\bar{2}$ 0 0) and ($\bar{2}$ 1 1 0) lattice planes. The black lines terminate at the position of dislocation cores (marked with arrows).[27] More detailed analysis is required to determine the degree of coherence of the interface and the exact nature of the dislocations. Fig. 11c shows a map of the local orientation of the lattice fringes, which indicates that atomic steps may be associated with each dislocation.

Another important feature common to the studied eutectics is a similar atomic stacking on both sides of the interface perpendicularly to the boundary and consisting of alternate cationic and anionic planes or layers with comparable atom density. A typical example is given on Fig. 12 for a corundum-fluorite interface with the orientation: $\{2\,\bar{1}\,\bar{1}\,0\}Al_2O_3//\{1\,0\,0\}ZrO_2$. The number of atoms indicated on Fig. 12 for each layer (or double-layer) is relative to a coincidence site lattice defined for this interface with the following dimensions: 4.12 nm × 2.60 nm for alumina and 4.11 nm × 2.57 nm for zirconia $10 \times d_{1010} = 4.12\,\text{nm} \approx 8 \times a(ZrO_2) = 4.11\,\text{nm}$ and $2 \times d_{0001} = 2.60\,\text{nm} \approx 5 \times a(ZrO_2) = 2.57\,\text{nm}$. The distances between two consecutive metal–oxygen layers along the direction perpendicular to the interface are not very different and this situation satisfies electroneutrality and bond length requirements at the interface.

## 5. Conclusions

Simultaneous crystallization of two oxides at a controlled rate gives rise to interphase boundaries with a low—and probably minimal—interfacial energy. HREM observations of interfaces in aligned eutectics, demonstrate that structures like fluorite, corundum or rocksalt can fit along particular crystallographic planes. Similarly to the coincidence site lattice for a grain boundary, an approximate coincidence lattice can be defined for each heterophase interface. The residual lattice mismatch amounts to a few per cent only and is accommodated by misfit dislocations or steps. Another feature common to all interfaces under consideration is the stacking sequence on both sides of the interface, which generally consists of alternate cationic and anionic planes or layers. Local electroneutrality at the interface and compatible interatomic distances generally result from this stacking despite their being quite different structures are facing each other. Crystallographic relationships and interface orientations seem to be controlled by the presence of densely packed oxygen planes.

Concerning potential thermomechanical properties, in particular strength at high temperature and creep resistance,

some important features of these melt grown composites are promising for using in mechanical engineering at very high temperature in the future:

- interfaces are coherent with a minimal interface energy as opposed to the grain boundaries present in sintered materials which usually correspond to high energy interfaces with a high grain boundary dislocation density;
- the oriented, elongated or interlocked microstructures consist of a continuous network of two single-crystal phases homogeneously distributed in the material without segregation and without grain boundary;
- no intermediate phase (like an amorphous phase) was observed at the interfaces which generally leads to a reduction in the strength at high temperature.

## References


1. Hulse, C. O. and Batt, J. A., Effect of eutectic microstructures on the mechanical properties of ceramic oxides. Final Technical Report UARL-N910803-10, May 1974. NTIS AD-781995/6GA, 140 p.
2. Argon, A. S., Yi, J. and Sayir, A., Creep resistance of directionally solidified ceramic eutectics of $Al_2O_3$/c-$ZrO_2$ with sub-micron columnar morphologies. *Mater. Sci. Eng. A*, 2001, **319–321**, 838–842.
3. Pastor, J. Y., Poza, P., Llorca, J., Pena, J. I., Merino, R. I. and Orera, V. M., Mechanical properties of directionally solidified $Al_2O_3$–$ZrO_2$ ($Y_2O_3$) eutectics. *Mater. Sci. Eng. A*, 2001, **308**, 241–249.
4. Michel, D., Perez y Jorba, M. and Collongues, R., Growth from skull-melting of zirconia-rare earth oxide crystals. *J. Crystal Growth*, 1978, **43**, 546–548.
5. Michel, D., Rouaux, Y. and Perez y Jorba, M., Ceramic eutectics in the system $ZrO_2$–$Ln_2O_3$: unidirectional solidification, microstructural and crystallographic characterization. *J. Mater. Sci.*, 1980, **15**, 61–66.
6. Revcolevschi, A., Arc image furnace for X-ray diffraction studies to 3000 °C and high temperature crystal growth. *Rev. Int. Hautes Temp. Refract.*, 1970, **7**, 73–90.
7. Mollard, F. R. and Flemings, M. C., Growth of composites from the melt. *Trans. AIME*, 1967, **239**, 1526–1546.
8. Cooksay, D. J. S., Munson, D., Wilkinson, M. P. and Hellawell, A. H., Freezing of some continuous binary eutectic mixtures. *Phil. Mag.*, 1964, **10**, 745–769.
9. Minford, W. J., Bradt, R. C. and Stubican, V. S., Crystallography and microstructure of directionally solidified oxide eutectics. *J. Am. Ceram. Soc.*, 1979, **62**, 154–157.
10. Michel, D., Mazerolles, L., Dallas, J. P., Stucky, M. and Portier, R., Oriented eutectics $Al_2O_3$–$ZrO_2$ ($Y_2O_3$), obtained from directional solidification. In *Physical Chemistry of the Solid State*, ed. P. Lacombe. Elsevier, Amsterdam, 1984, pp. 397–404.
11. Tiller, W. A., *Liquid Metals and Solidification*. American Society for Metals, Metals Park, OH, 1958, pp. 279–318.
12. Hunt, J. D. and Jackson, K. A., Binary eutectic solidification. *Trans. AIME*, 1966, **236**, 843–852.
13. Ashbrook, R. L., Directionally solidified ceramic eutectics. *J. Am. Ceram. Soc.*, 1977, **60**, 428–435.
14. Stubican, V. S. and Bradt, R. C., Eutectic solidification in ceramic systems. In *Annual Review of Materials Science (Vol 11)*, ed. R. A. Huggins, R. H. Bube and D. A. Vermilya. Annual Review, Inc, Palo Alto, CA, 1981, pp. 265–297.
15. Tuohig, W. D. and Tien, T. Y., Susolidus phase equilibria in the system $ZrO_2$–$Al_2O_3$–$Y_2O_3$. *J Am. Ceram. Soc.*, 1980, **63**, 595–596.
16. Waku, Y., Nakagawa, N., Wakamoto, T., Ohtsubo, H., Shimizu, K. and Kohtoku, Y., A ductile ceramic eutectic composite with high strength at 1873 K. *Nature*, 1997, **389**, 49–52.
17. Waku, Y., Nakagawa, N., Wakamoto, T., Ohtsubo, H., Shimizu, K. and Kohtoku, Y., High temperature strength and stability of unidirectionally solidified $Al_2O_3$/YAG eutectic composite. *J. Mater. Sci.*, 1998, **33**, 1217–1225.
18. Frazer, C. S., Dickey, E. and Sayir, A., Crystallographic texture and orientation variants in $Al_2O_3$–$Y_3Al_5O_{12}$ directionally solidified eutectic crystals. *J. Crystal Growth*, 2001, **233**, 187–195.
19. Revcolevschi, A., Dalhenne, G. and Michel, D., Interfaces in directionally solidified oxide–oxide eutectics. In *External and Internal Interfaces of Metal Oxides*, ed. J. C. Dufour and J. Nowotny. Trans. Tech. Publications, Switzerland, 1988, pp. 173–197.
20. Michel, D., Mazerolles, L. and Portier, R., Crystallographic features of interfaces in zirconia eutectics. In *Zirconia Ceramics 6*, ed. S. Somiya. Ushida Rokakuo, Tokyo, 1986, pp. 45–48.
21. Mazerolles, L., Michel, D. and Portier, R., Interfaces in oriented $Al_2O_3$–$ZrO_2$ ($Y_2O_3$) eutectics. *J. Am. Ceram. Soc.*, 1986, **69**, 252–255.
22. Echigoya, J. and Suto, H., Structure of interphase interface and solute segregation in directionally solidified MgO–$ZrO_2$ eutectic. In *Proceedings of JIMIS-4 Grain Boundary Structure and Related Phenomena. Trans. Jpn. Inst. Metals Suppl.*, 1986, 213–220.
23. Kennard, F. L., Bradt, R. C. and Stubican, V. S., Directional solidification of the $ZrO_2$–MgO eutectic. *J. Am. Ceram. Soc.*, 1974, **57**, 428–431.
24. Hÿtch, M. J., Snoeck, E. and Kilaas, R., Quantitative measurement of displacement and strain fields from HREM micrographs. *Ultramicroscopy*, 1998, **74**, 131–146.
25. Snoeck, E., Warot, B., Ardhuin, H., Rocher, A., Casanove, M. J., Kilaas, R. *et al.*, Quantitative analysis of strain fields in thin films from HRTEM micrographs. *Thin Solid Films*, 1998, **319**, 157–162.
26. Hÿtch, M. J., Vermaut, P., Malarria, J. and Portier, R., Study of atomic displacement fields in shape memory alloys by high-resolution electron microscopy. *Mater. Sci. Eng. A*, 1999, **273–275**, 266–270.
27. Hÿtch, M. J., Putaux, J.-L. and Pénisson, J.-M., Measurement of the displacement field around dislocations to 0.03 Å by electron microscopy. *Nature*, 2003, **423**, 270–273.